MAPPING AND ASSESSMENT OF THE SPATIAL AND TEMPORAL DISTRIBUTION OF TURBIDITY IN LAKE BUHI FROM SENTINEL-2 IMAGES USING GEOGRAPHICALLY WEIGHTED REGRESSION AND NORMALIZED DIFFERENCE TURBIDITY INDEX

K.A.N. Amaro[1*], L.M.G. Cortez[1], J.M. Medina[1,2], A.C. Blanco[1,2,3]

[1] Department of Geodetic Engineering, University of the Philippines Diliman, Quezon City, Philippines – (knamaro, lgcortez1,jmmedina, acblanco)@up.edu.ph
[2] Training Center for Applied Geodesy and Photogrammetry, University of the Philippines Diliman, Quezon City, Philippines
[3] Space Information Infrastructure Bureau, Philippine Space Agency, Quezon City, Philippines – ariel.blanco@philsa.gov.ph

KEY WORDS: NDTI, regression, water quality, turbidity models, ACOLITE.

ABSTRACT:

Water quality monitoring is vital in ensuring the suitability of Lake Buhi for aquaculture and recreational activities. However, with the limitations of traditional monitoring methods, the Bureau of Fisheries and Aquatic Resources (BFAR) cannot comprehensively characterize the spatial and temporal water quality patterns in the lake. With the development of remote sensing methods, this study aimed to describe the spatial and temporal variability of turbidity in Lake Buhi in 2020 using Geographically Weighted Regression (GWR) and the Normalized Difference Turbidity Index (NDTI) applied to Sentinel-2 images. GWR provided accurate estimates of turbidity, with the results achieving an R^2 value of 0.98 for the February image and 0.93 for October. GWR-derived turbidity was used as an alternative to in situ data and then regressed with NDTI values to acquire turbidity models for dry and wet seasons. Upon validation, the best turbidity model for the dry (R^2 = 0.59, RMSE=0.60, MAE=0.15) and wet (R^2 = 0.49, RMSE = 1.22, MAE = 0.25) seasons produced acceptable results, hence, used to assess the spatial and temporal variability of turbidity in the lake throughout 2020. The analysis revealed that Lake Buhi is more turbid during the dry season than the wet season. Turbidity during the dry season is governed by its natural water flow, while it is heavily influenced by precipitation during the wet season.

1. INTRODUCTION

Water quality monitoring is an essential part of water resource management as it allows for the early detection of existing and emerging problems, the identification of trends in water quality, and the provision of information for developing management strategies and regulations. It is mostly employed through conventional methods, which continue to face the challenges of being an intensive and costly procedure (Zainurin et al., 2022).

The Bureau of Fisheries and Aquatic Resources (BFAR) Region V implements the conventional method of acquiring water quality data in Lake Buhi, which is located in Buhi, Camarines Sur, Philippines. In 2020, the lake was only sampled for three months because of the constraints brought about by the COVID-19 pandemic and poor weather conditions. Furthermore, only seven sampling points were monitored for each of these months. The number of in-situ measurements from these field surveys would not be sufficient to describe and understand the overall conditions of the lake.

With the limitations of the traditional methods, the study aimed to introduce a method that would complement the existing data for turbidity. Turbidity is an important water quality parameter because it tells us about the amount of dissolved oxygen (EPA, 2021) and the primary productivity of water as it limits light penetration (Baughman et al., 2015).

This study aimed to characterize the spatial and temporal variability of turbidity in Lake Buhi in 2020 using Sentinel-2 images and NDTI. Specifically, the study estimated the true turbidity in the lake using GWR. Then, the GWR-estimated turbidity was regressed against NDTI values to develop turbidity models for the dry and wet seasons. The models' performance was assessed using the coefficient of determination, R^2, Root Mean Square Error (RMSE), and Mean Absolute Error (MAE). Turbidity maps were generated and used to describe the spatial and temporal turbidity distribution in the lake.

The results of this study can provide useful information for understanding the spatial and temporal variability of turbidity in the lake that cannot be fully provided by the limited in-situ data available from BFAR for 2020. The assessment of the spatial and temporal variation of turbidity in 2020 could aid the governing body of Water Quality Management Area (WQMA), Department of Environment and Natural Resources - Environmental Management Bureau (DENR-EMB), and BFAR in understanding the conditions of the lake.

2. METHODOLOGY

2.1 Study Area

Lake Buhi (Figure 1), located in Buhi, Camarines Sur, Philippines, covers an area of approximately 1335 ha (EMB Region V, 2022). It is primarily used for fish farming and as a sanctuary for Sinarapan. It has 14 tributaries (Binoya et al., 2008), including the Iraya River and Sta. Cruz River, that feeds water, nutrients, and sediments into the lake. The Tabao River, located in the southwestern part of the lake, is the only river that flows outward. Thus, the general flow of the water in the lake is

from the eastern part, where the major inlets are located, towards the southwestern part.

Lake Buhi watershed was designated as a WQMA in 2013. As such, concerned agencies are mandated to closely monitor the lake to prevent its degradation.

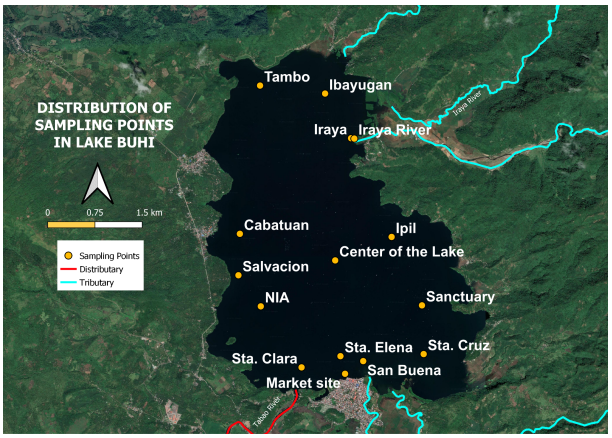

Figure 1. Distribution map of sampling stations of BFAR Region V, some of the tributaries, and the only distributary in Lake Buhi.

2.2 Data Requirements

2.2.1 In situ data

In-situ turbidity data were obtained from BFAR Region V. They measure turbidity and other water quality parameters in 15 stations that are used for aquaculture purposes (see Figure 1). Each station harbors fish cages, thus, when Buhi Local Government Unit (LGU) reduced the fish cages, the number of stations also decreased, leading to a minimum of seven sampling stations observed starting September 5, 2019.

They measure turbidity at three depths: surface, middle, and bottom. Turbidity values are in the Nephelometric Turbidity unit (NTU), where higher values signify higher turbidity. In this study, only the surface measurements were used.

2.2.2 Sentinel-2 images

Sentinel-2 L1C images have 13 spectral bands from VNIR to SWIR in 10 to 60 m spatial resolutions. It has a swath width of 290 km and a revisit frequency of 5 days. Sentinel-2 L1C images with a similar sensing date as the field survey of BFAR in 2020 were downloaded from the Copernicus Open Access Hub.

In 2020, field surveys were conducted on the following dates: February 18, May 28, and October 8. This study only focused on 2020 as it provided the most usable and with the lowest cloud cover images. An allowance of ±5 days between the satellite overpass and in-situ sampling is desired to minimize the possible errors due to the temporal variation of turbidity in the lake. However, the available usable Sentinel-2 images for the lake do not permit the strict employment of such restriction. Only the image for February follows this restriction.

To acquire images for May and October, all images within these months were inspected for suitability (i.e., lowest cloud cover). The date with the lowest cloud cover was chosen. The downloaded satellite image in May differs by 19 days from the date of the in-situ sampling. Such a time difference may already have an adverse effect on the accuracy of the results. Meanwhile, the satellite image acquired for October has an 8-day difference from the date of in-situ sampling. Despite the relatively shorter time difference, it should be noted that the Philippine Atmospheric, Geophysical, and Astronomical Services Administration (PAGASA) reported a tropical depression named Ofel on October 13, 2020, that caused tropical cyclone wind signal (TCWS) No. 1 to be hoisted in Camarines Sur and other provinces. Thus, the occurrence of tropical depression Ofel was noted in assessing the accuracy of the results.

To characterize the turbidity of Lake Buhi in 2020, the satellite image with the lowest cloud cover for the other months was downloaded. No restriction on the date was implemented as the result of these months will not be compared to any in-situ measurements. No image was acquired in September 2020 due to high cloud coverage for all available satellite images. The peak typhoon season in the Philippines is from July until October when at least two typhoons enter the Philippine Area of Responsibility (PAR). Particularly, three tropical cyclones entered the PAR during September 2020 (PAGASA, 2023), which can be the reason why there is high cloud coverage for all available images in this month.

2.3 Data Processing

Figure 2 shows the overview of the entire methodology of estimating turbidity, assessing the methods' accuracy, and mapping the results.

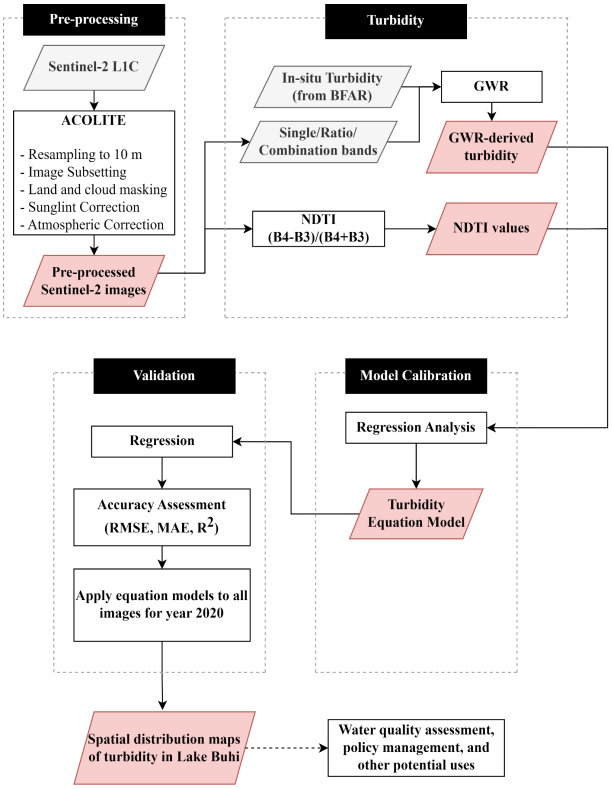

Figure 2. Methodological workflow for mapping turbidity in Lake Buhi using Sentinel-2 data.

2.3.1 Pre-processing of Sentinel-2 images

ACOLITE is an algorithm processor tailored by the Royal Belgian Institute of Natural Sciences (RBINS) for marine, coastal, and inland waters and does not require in-situ atmospheric data to conduct atmospheric correction (Vanhellemont & Ruddick, 2016). Furthermore, ACOLITE performs atmospheric correction using the Dark Spectrum Fitting (DSF) algorithm that is specifically developed for satellites used in water applications, such as Landsat-8 and S2 satellites. DSF has been proven to perform well in turbid and productive waters and clear waters (Vanhellemont & Ruddick, 2018).

Eleven Sentinel-2 L1C images from 2020 were pre-processed using ACOLITE. Processes such as resampling, image subsetting, land and cloud masking, sunglint correction, and atmospheric correction were conducted through the ACOLITE software. Default settings of ACOLITE were used except for sunglint correction.

Images were resampled to 10 m and subset according to the geographic coordinates that cover the study area. The "dsf_residual_glint_correction" was manually set to true in the settings file. We used the default settings for all related settings for masking and sun glint correction. Along with the rhot files from the top of atmosphere reflectance and rhos files from earth surface reflectance, we also obtained the remote sensing reflectance (sr^{-1}) for water pixels by specifying "Rrs_*" in the "L2W parameter" option of the ACOLITE interface. Using SNAP, all outputs were reprojected to WGS 84/ UTM zone 51N to accurately facilitate distance components of the GWR function.

2.3.2 Deriving NDTI values

The Normalized Difference Turbidity Index (NDTI) uses the green (B3) and red (B4) bands. This index works under the assumption that if the turbidity level increases, it is expected that the reflectance of the red band will be greater than that of the green band. Using the derived remote sensing reflectance (Rrs), NDTI maps were generated through SNAP's Band Math Tool using the equation established by Lacaux et al. (2007):

$$NDTI = \frac{Rrs_{red} - Rrs_{green}}{Rrs_{red} + Rrs_{green}} \quad (1)$$

where Rrs_{red} = remote sensing reflectance for Band 4
Rrs_{green} = remote sensing reflectance for Band 3

2.3.3 GWR Turbidity Estimation

With inadequate in situ data, the study explored the applicability of GWR-derived turbidity as the alternative for in-situ turbidity. We used GWR for estimating the true turbidity because it can provide reliable and accurate estimates even with only a few points (Chu et al., 2018).

GWR is a regression technique that extends global regression into local relationships between the independent variable and dependent variables at different locations. The idea of GWR is represented by the model (Sulekan & Syed Jamaludin, 2020):

$$y_i = \beta_0(u_i, v_i) + \sum_k \beta_k(u_i, v_i)x_{ik} + \varepsilon_i \quad (2)$$

where (u_i, v_i) = coordinates of i^{th} point in space

$\beta_k(u_i, v_i)$ = realization $\beta_k(u, v)$ at point i

Observations nearby i were weighted more than those further away, that is:

$$\hat{\beta}(u_i, v_i) = (\boldsymbol{X}^T\boldsymbol{W}(u_i, v_i)\boldsymbol{X})^{-1}\boldsymbol{X}^T\boldsymbol{W}(u_i, v_i)\boldsymbol{y} \quad (3)$$

where $\hat{\beta}$ = estimate of β
$\boldsymbol{W}(u_i, v_i)$ = matrix of n by n with zero as off-diagonal elements and the geographically weighted of observed data for point i as diagonal elements

In this study, GWR spatial-analysis regression was implemented through MATLAB using the 2021 version of the Econometrics Toolbox of Dr. James P. LeSage. Three weighting methods can be employed from this toolbox: gaussian, exponential, and tri-cube. Gaussian and exponential methods use user-specified or function-computed distance-based measures in determining the neighboring pixels that will be used in establishing the local regression equation. In contrast, the tri-cube weighting method employs the nearest-neighbor measure (LeSage, 1999). In LeSage's toolbox, a distance-based measure for Gaussian and exponential methods is called bandwidth. In this study, the default Gaussian weighting method was employed because it has the least processing time among the three methods. To account for the varying spatial density of each satellite image, the computed optimal bandwidth from the GWR function was used in the turbidity estimation for each image.

In performing the regression, in-situ turbidity was the dependent variable, while all S2 bands, ratio bands, and their combinations adopted from various studies, as shown in Table 1, were used as the independent variables. The study also assessed the use of two explanatory variables, specifically B4 in combination with the bands in Table 1. B4 was used in several studies and showed satisfactory results using this band in estimating turbidity. GWR results with a high R^2, low RMSE, and MAE, and no negative turbidity values were considered in the model calibration.

2.3.4 Model Calibration and Accuracy Assessment

GWR-derived turbidity values were used as the true turbidity in establishing a model that relates NDTI to the in-situ turbidity. Thus, the NDTI values and GWR-derived turbidity were used as the independent and dependent variables, respectively.

In the regression analysis, 100 distributed and randomly selected points across Lake Buhi were used. The points were divided into a 7:3 ratio, 70% for calibration and 30% for validation. For the calibration of the mathematical model, the study also evaluated linear and non-linear regression (exponential) models and different pixel aggregation methods (no aggregation, median, and mean). The accuracy of the models was evaluated using RMSE, MAE, and R^2.

The calibrated models that provided the highest R^2 and lowest RMSE and MAE for each dry and wet season determine the equation in estimating turbidity from NDTI values. A turbidity model was generated for the dry and wet seasons since it was established in several studies that seasonal changes affect turbidity.

Ratios/ Combinations	Reference	Result
B1/B3	Orlandi et al. (2018)	R^2= 0.96
B8a/B3	Hussein et al. (2022)	R^2 = 0.78
B2/B3	Assegide et al. (2023)	R^2 = 0.86
B4/B3		R^2 = 0.92
B2/B4		R^2 = 0.89
B3+B5	Ma et al. (2021)	r = 0.83
B3*B5		r = 0.83
(B3*B5)/(B4+B12)		r = 0.86
(B3+B5)/(B2/B3)		r = 0.80

Table 1. Band ratios and combinations used for turbidity estimation using GWR.

2.3.5 Spatial and Temporal Analysis

The turbidity models for the dry season and the wet season were applied to pre-processed Sentinel-2 images. We then normalized the data using Equation 4 to facilitate the comparison of turbidity throughout 2020. Maps were created for the spatial analysis using QGIS v3.16.13. Meanwhile, a line chart showing the turbidity values throughout 2020 was generated for the temporal analysis of turbidity.

$$X_{new} = \frac{X - X_{min}}{X_{max} - X_{min}} \quad (4)$$

where X = estimated turbidity value
X_{min} = lowest turbidity value
X_{max} = highest turbidity value

3. RESULTS

3.1 In-situ turbidity of Lake Buhi

The average turbidity recorded in Lake Buhi from 2018 to 2021 is presented in Figure 3. The lake's average turbidity ranges from 1.83 to 4.52 NTU, with the maximum and minimum average turbidity occurring on September 05, 2019, and October 8, 2020, respectively.

We downloaded the satellite images with a 5-day difference from the sampling dates of BFAR from 2018 to 2021. Due to the presence of clouds, only 15, 14, and 8 points were acquired for 2018, 2019, and 2020. No usable image was acquired for the year 2021. Using these available points, R^2 values of 0.0280, 0.0866, and 0.0003 were acquired for 2018, 2019, and 2020 by linearly regressing the NDTI values with in-situ turbidity measurements.

The points from BFAR alone could not provide reliable and acceptable models for estimating turbidity. Due to this, we conducted a water sampling field survey on March 25, 2023, to supplement the available in-situ data from BFAR. However, because of a technical problem with the SD card of the CLW instrument, we failed to retrieve the in-situ measurements. The lack of sufficient data compelled us to employ GWR to estimate the true turbidity as it allows accurate and reliable estimation even with the use of a few points (Chu et al., 2018). The GWR-derived turbidity was used as the true turbidity for the succeeding processes.

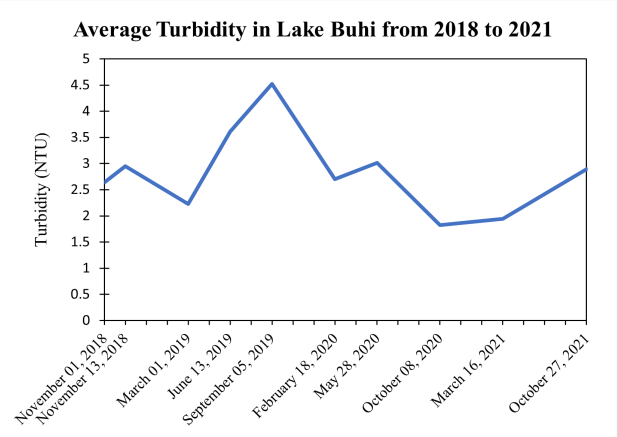

Figure 3. The average turbidity of Lake Buhi from 2018 to 2021 based on the field data from BFAR Region V.

3.2 GWR-derived turbidity models

Out of the seven available in-situ turbidity points for each month, only five for February, three for May, and four for October have matched points in the pre-processed satellite image. Due to the lack of data points, illogical results were acquired for May, specifically an extremely high value of R^2 or mostly a value of 1, indicating a perfect prediction. It is only fitting to not use the image for May because of the large difference between the sampling and satellite overpass dates. Hence, the study focused on acquiring GWR estimates for February and October, respectively, representing dry and wet months.

For February, five data points were enough to estimate turbidity using one and two explanatory variables. However, the four points for October can only be used in estimating turbidity using one explanatory variable. To allow the estimation using two explanatory variables for October, a pixel closest to Sta. Elena's location was considered. A pixel closest to Sta. Elena's location was added for October and bore its turbidity value. The distribution of these points ensures that all parts of the lake are well-represented in GWR processing.

By using one explanatory variable, an R^2 up to 0.632 was achieved for February. For October, 10 variables obtained an R^2 greater than 0.8, and up to 0.973 was achieved. Meanwhile, when two explanatory variables were used, five variables for February and two for October achieved an R^2 greater than 0.8. The highest R^2 achieved using two explanatory variables for February and October were 0.986 and 0.979, respectively.

Among all the examined GWR models, only those with R^2 greater than 0.8, low RMSE and MAE, and non-negative turbidity values were selected for calibration (See Table 2).

	Explanatory variables	R^2	RMSE	MAE
February	B4, B8a/B3	0.986	1.758	1.480
	B4, B2/B4	0.814	2.998	2.474
	B4, (B3*B5)/ (B4+B12)	0.815	0.888	0.697
	B4, (B4+B5)/ (B2/B3)	0.934	8.479	6.976
October	B1/B3	0.894	4.013	2.147
	B4, B4/B3	0.934	1.886	1.352

Table 2. GWR models with R^2 greater than 0.8 and were used for calibration.

We explored the linear and exponential regression of the non-aggregated, median, and mean NDTI and GWR-derived turbidity for calibration. The result showed that the combination of B4 and (B4+B5)/(B2/B3) consistently achieved the highest R^2 for February (0.45 for non-aggregated, 0.58 for mean, and 0.57 for median values). For October, the combination of B4 and B4/B3 attained the highest R^2 (0.08 for non-aggregated, 0.22 for mean, and 0.19 for median values).

3.3 Regression Modeling of NDTI and GWR-derived Turbidity

The calibrated models that achieved the highest R^2 were validated. The result showed that Equation 5 achieved the highest R^2 RMSE, and MAE for February (R^2=0.55, RMSE=0.60, and MAE=0.15). On the other hand, the highest R^2 and RMSE were achieved using Equation 6 for October (R^2 =0.49, RMSE=1.22, and MAE=0.25).

These equations were used as final models to estimate turbidity from NDTI values for the dry and wet seasons, respectively:

$$Turbidity = -4.2232 \times NDTI - 0.0626 \quad (5)$$

$$Turbidity = 4.2787 \times e^{1.4014 \times NDTI} \quad (6)$$

where $Turbidity$ is measured in NTU.

3.4 Spatial and Temporal Analysis of Turbidity in Lake Buhi

Turbidity maps (Figure 4) show the spatial distribution of turbidity throughout Lake Buhi. The low-to-high scale is a relative scale that allows easy inspection of areas that have lower or higher turbidity values compared to other areas. Only eight images provided good coverage of the lake that will allow for proper analysis of the spatial distribution of turbidity.

PAGASA divided the climate of the country into two seasons: dry and rainy seasons. The dry season occurs from December to May, while the rainy season is from June to November. This division was adopted in describing the temporal variation of turbidity in the lake.

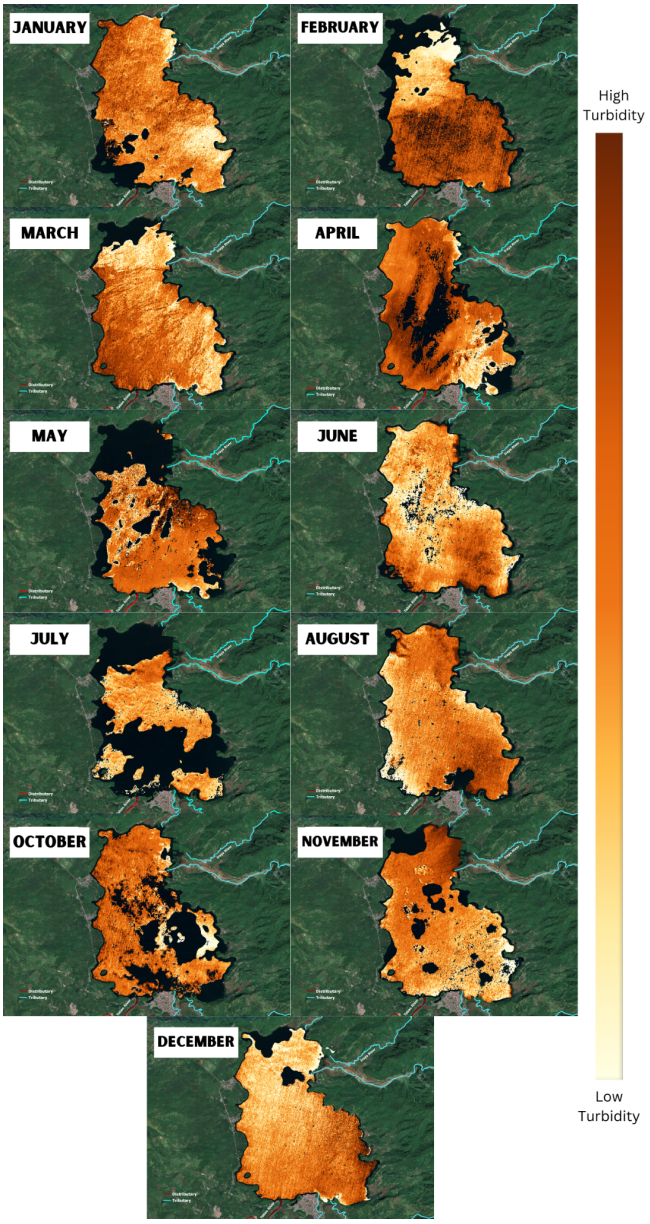

Figure 4. Turbidity maps for Lake Buhi in 2020. No usable satellite image was downloaded for September. The black areas represent the masked clouds and cloud shadows.

The turbidity values in the lake range from 0.98 to 4.18 NTU during the dry season. In December, the turbidity ranges from 1.08 to 2.94 NTU, where the turbidity generally increases from the northern to the southern area. In January, the turbidity ranges from 1.05 to 3.26 NTU, with the western lake generally having relatively higher values compared to the east. In February, the turbidity values became more varied, with values ranging from 0.98 to 4.18 NTU. The inlet of the lake from the Iraya River (north-eastern river) showed lower turbidity compared to the southern part with higher turbidity values. Turbidity in March ranges from 1.49 to 3.74, where it can be

observed that the northernmost and eastern parts of the lake have lower turbidity, while the southern and western parts of the lake have higher turbidity. Meanwhile, turbidity ranges from 1.60 to 4.09 NTU in April and 1.59 to 4.17 NTU in May.

During the wet season, the turbidity ranges from 1.05 to 2.84 NTU. In June, the turbidity ranges from 1.05 to 2.17 NTU with relatively higher turbidity values observed in areas near the shore and in the southwest area where the fish sanctuary is located. The turbidity in July ranges from 1.05 to 2.28 NTU and 1.05 to 2.83 NTU in August. Higher turbidity in August can be observed in the northeastern and southeastern areas of the lake where the major inlets are located. In October, the turbidity ranges from 1.62 to 2.67 NTU, with relatively high turbidity values observed throughout the lake. Lastly, the turbidity in November ranges from 1.62 to 2.67 NTU, with turbidity gradually decreasing from the north to the south area of the lake.

To examine the temporal variation of turbidity, the mean, median, and P90 threshold values per image were plotted in a line chart (Figure 5). Generally, we observed that the turbidity is higher during the dry season. Peaks were observed during February and May, while troughs during March and June.

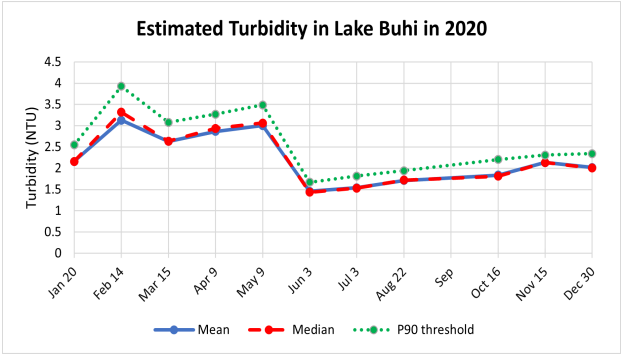

Figure 5. Mean, median, and P90 threshold of the turbidity in Lake Buhi in 2020, estimated from the established turbidity models.

4. DISCUSSION & CONCLUSION

Acquiring cloud-free images over water bodies has been a challenge for us, as well as for other water quality studies including Li et al. (2021). Despite this issue, we were able to study the turbidity of Lake Buhi with the help of more advanced remote sensing and mathematical techniques.

ACOLITE proved its suitability in pre-processing Sentinel-2 images even without data about the lake, as shown in this study and other water quality studies (Caballero et al., 2020). This atmospheric correction method successfully removed clouds and sunglints but failed to remove cloud shadows and unwanted streaks. Cloud shadows should be identified and removed, if possible, as this can negatively affect the succeeding processes, such as estimating water quality parameters. The streaks observed in the images were attributed to systematic or internal errors in the sensors. The Data Quality Report-L1C MSI of the S2 MSI ESL Team in 2022 identified several product anomalies on Sentinel-2 L1C images. Corrections for such errors are not within the capabilities of ACOLITE.

GWR showed its capability to estimate turbidity even using only five points. GWR achieved an R^2 as high as 0.98 using two explanatory variables for February, while it achieved an R^2 as high as 0.97 using one and two explanatory variables for October. Most variables that achieved an R^2 greater than 0.8 include the bands B3, B4, and B5. This result is consistent with several studies. The findings of Maimouni (2022) indicate that B3 and B4 have a highly significant relationship with in-situ turbidity, with B4 obtaining the strongest correlation coefficient of 95% and an R^2=0.89. Pisanti (2022) further demonstrated the potential of B3 and B4, and B2 as well, as they showed a good correlation with the in-situ data. Meanwhile, Sebastiá-Frasquet (2019) found B5 suitable for identifying turbidity patterns in inland waters.

In the absence of sufficient in-situ turbidity data, GWR-derived turbidity can be used as an alternative. Due to its satisfactory results, GWR can be used to estimate turbidity instead of linear regression, especially if in-situ data is available. Chu et al. (2018) showed the superiority of GWR over linear regression in estimating turbidity because it takes into consideration the spatial variability of turbidity throughout the water body.

Estimating turbidity from Sentinel-2 using NDTI can provide relatively good estimates, achieving R^2=0.57 for the dry season and R^2=0.22 for the wet season. Relatively lower R^2 can be attributed to the 8-day difference between the satellite overpass and field survey dates and the occurrence of a tropical depression within that timeline. Perrone et al. (2021) found no negative effect on the accuracy of their predictive models using such a time window, however, only under stable weather conditions.

Using the established turbidity models, this study confirmed that the turbidity in Lake Buhi is low and within acceptable standards based on the criteria of the Alaska Department of Environmental Conservation (2016) of less than 5 NTU. This criterion is being adopted by BFAR Region V in assessing the acceptability of the turbidity concentration in the lake. The standard deviation (SD) for the data in Figure 3 is 0.846. Generally, data with SD values less than 1 are considered to have low variation. Thus, the turbidity in the lake can be considered low and invariable across time.

With the use of the turbidity maps, we found that the turbidity in the lake is higher during the dry season than in the wet season. Lower turbidity during the wet season can be explained by the higher water level (Li & Xia, 2023) and enhanced water exchange (Liu et al., 2023) which decreases the sediment settlement and resuspension.

During the dry season, the spatial distribution of turbidity in Lake Buhi is governed by the general flow of the water. The turbidity is relatively low in the inlets (northeast and southwest areas), while it is higher near the outlet (southwest part of the lake). Lower turbidity near the inlets can be explained by the low river flow rate during the dry season which does not cause the suspended materials to be stirred up from the lake bed (Swenson et al., 2018). Relatively high turbidity near the mouth of the Tabao River can be attributed to the natural flow of the water that causes the sediments to build up near this area. Another possible factor for the higher turbidity in the southern area is the land use/land cover of the area. Vegetation reduces the occurrence of soil erosion, which causes higher concentrations of suspended solids in the water and thus,

decreases turbidity. Meanwhile, urban areas increase pollution due to industrial and domestic waste which contributes to the increase of water turbidity (Li & Xia, 2023).

The distribution of turbidity during the wet season is highly influenced by the increased precipitation that increases the water exchange, transport, and consequently, turbidity (Liu et al., 2023). High water exchange and transportation explain the reduced turbidity variation during this season. We also consistently observed higher turbidity values in the northeastern area of the lake, where the confluence of the Iraya River and the lake can be found. This can be attributed to an increased flow rate during the wet season, which can cause suspended materials to be stirred up from the lake or river bed.

Fish cages are located in the northern area of the lake and a fish sanctuary for Sinarapan repopulation is found in the southeastern part. We did not observe any particular pattern of turbidity distribution in these areas. A similar observation was shown in the study of Osei et al. (2019) where there was no significant difference between the turbidity in areas with or without fish cages. This led us to conclude that the effect of fish cages and sanctuaries on the turbidity in the lake may be insignificant.

Overall, the use of GWR and NDTI in estimating turbidity from Sentinel-2 images achieved relatively good results that can be used to complement the presently available data and to further improve our understanding of the spatial and temporal variation of turbidity and other water quality parameters in Lake Buhi.

The spatial and temporal observations could be further enhanced if the available images provided good coverage of the lake and covered all months of the year. The suitability of Landsat-8 or the fusion of Landsat-8 and Sentinel-2 for providing such images can be explored in future studies.

Turbidity estimates could also be improved if enough in-situ turbidity data was available and satellite images were synchronized with the field survey dates. With this, we recommend that the monitoring of the lake be conducted on or close to the day of the Sentinel-2 or other sensor's overpass. If possible, the study also recommends that the lake be monitored at least once a month or more, especially in the occurrence of extreme weather disturbances and fish kills, to capture the variation in water quality brought about by these events. The Manual on Ambient Water Quality Monitoring issued through EMB Memorandum Circular 2008-008 already requires a sampling frequency of 10 months in a year for primary parameters, such as Total Suspended Solids, for trend monitoring. Additional and adjusted monitoring would be a great help in improving the reliability of studies exploring trends in water quality.

Supplemental information about the hydrodynamics and bathymetry of the lake can further improve the reliability of the assessment. Also, the effect of rainfall on the turbidity patterns of the lake can be better understood with the use of precipitation data.

ACKNOWLEDGEMENTS

We would like to extend our gratitude to BFAR Region V for providing us with their available in-situ turbidity data and sharing with us the methods they employ to acquire water data from Lake Buhi. Buhi LGU and CENRO Iriga City Buhi Wildlife Sanctuary also provided their assistance for the conduct of our field survey in the lake.

REFERENCES

Alaska Department of Environmental Conservation. (2016, September 9). *Listing Methodology for Determining Water Quality Impairments from Turbidity GUIDANCE FINAL September 9, 2016 Alaska Department*. Alaska Department of Environmental Conservation. Retrieved from https://dec.alaska.gov/media/16352/turbidity-listing-methodology-final-09-09-2016.pdf

Assegide, E., Shiferaw, H., Tibebe, D., Peppa, M. V., Walsh, C. L., Alamirew, T., & Zeleke, G. (2023). Spatiotemporal Dynamics of Water Quality Indicators in Koka Reservoir, Ethiopia. *Remote Sensing*, 15(4), 1155. https://doi.org/10.3390/rs15041155

Baughman, C., Jones, B., Bartz, K., Young, D., & Zimmerman, C. (2015). Reconstructing Turbidity in a Glacially Influenced Lake Using the Landsat TM and ETM+ Surface Reflectance Climate Data Record Archive, Lake Clark, Alaska. In *Remote Sensing* (Vol. 7, Issue 10, pp. 13692–13710). MDPI AG. https://doi.org/10.3390/rs71013692

Binoya, C. S., dela Trinidad, J. V., Estrella, A. B., Llesol, C. B., & Osea, G. B. (2008). Managing and Conserving Lake Buhi An Agroecosystems Analysis for Sustainable Development. SEARCA.

Caballero, I., Román, A., Tovar-Sánchez, A., & Navarro, G. (2022). Water quality monitoring with Sentinel-2 and Landsat-8 satellites during the 2021 volcanic eruption in La Palma (Canary Islands). Science of The Total Environment, 822, 153433. https://doi.org/10.1016/j.scitotenv.2022.153433

Chu, H. J., Kong, S. J., & Chang, C. H. (2018). Spatio-temporal water quality mapping from satellite images using geographically and temporally weighted regression. *International Journal of Applied Earth Observation and Geoinformation, 65*, 1–11. https://doi.org/10.1016/J.JAG.2017.10.001

EMB V. (2022). 2021 Regional State of the Brown Environment Report. Retrieved from https://r5.emb.gov.ph/wp-content/uploads/2022/06/EMB-5-2021-Regional-Annual-State-of-Brown-Environment-Report.pdf

EPA. (2021, July). Factsheet on Water Quality Parameters. https://www.epa.gov/system/files/documents/2021-07/parameter-factsheet_turbidity.pdf

Hussein, N. M., Assaf, M. N., & Abohussein, S. S. (2023). Sentinel 2 analysis of turbidity retrieval models in inland water bodies: The case study of Jordanian dams. *The Canadian Journal of Chemical Engineering, 101(3)*, 1171–1184. https://doi.org/10.1002/cjce.24526

Lacaux, J. P., Tourre, Y. M., Vignolles, C., Ndione, J. A., & Lafaye, M. (2007). Classification of ponds from high-spatial resolution remote sensing: Application to Rift Valley Fever epidemics in Senegal. *Remote Sensing of Environment, 106*(1), 66–74. https://doi.org/10.1016/j.rse.2006.07.012

Lesage, J. P. (1999). *The Theory and Practice of Spatial Econometrics*. https://www.spatial-econometrics.com/html/sbook.pdf

Li, X., Ling, F., Cai, X., Ge, Y., Li, X., Yin, Z., Shang, C., Jia, X., & Du, Y. (2021). Mapping water bodies under cloud cover using remotely sensed optical images and a spatiotemporal dependence model. In *International Journal of Applied Earth Observation and Geoinformation* (Vol. 103, p. 102470). Elsevier BV. https://doi.org/10.1016/j.jag.2021.102470

Li, J., & Xia, C. (2023). Drivers of Spatial and Temporal Dynamics in Water Turbidity of China Yangtze River Basin. *Water, 15*(7), 1264. https://doi.org/10.3390/w15071264

Liu, X., Xia, J., Zu, J., Zeng, Z., Li, Y., Li, J., Wang, Q., Liu, Z., & Cai, W. (2023). Spatiotemporal variations and gradient functions of water turbidity in shallow lakes. *Ecological Indicators, 147,* 109928. https://doi.org/10.1016/j.ecolind.2023.109928

Ma, Y., Song, K., Wen, Z., Liu, G., Shang, Y., Lyu, L., Du, J., Yang, Q., Li, S., Tao, H., & Hou, J. (2021). Remote Sensing of Turbidity for Lakes in Northeast China Using Sentinel-2 Images With Machine Learning Algorithms. *IEEE Journal of Selected Topics in Applied Earth Observations and Remote Sensing, 14*, 9132–9146. https://doi.org/10.1109/JSTARS.2021.3109292

Maimouni, S., Moufkari, A. A., Daghor, L., Fekri, A., Oubraim, S., & Lhissou, R. (2022). Spatiotemporal monitoring of low water turbidity in Moroccan coastal lagoon using Sentinel-2 data. *Remote Sensing Applications: Society and Environment, 26*, 100772. https://doi.org/10.1016/J.RSASE.2022.100772

Nieves, P. M., Mendoza, A. B., Rey, S., & Bradecina, B. (2020). Occurrence and recurrence: the fish kill story in Lake Buhi, Philippines (Vol. 13, Issue 1). http://www.bioflux.com.ro/aacl

Olaño, V. L., & Montojo, U. (2005). Investigation of massive fish kill in Lake Buhi, Camarines Sur, Philippines. SEAFDEC/AQD Institutional Repository Home. https://repository.seafdec.org.ph/handle/10862/6151

Orlandi, M., Silvio Marzano, F., & Cimini, D. (2018). Remote sensing of water quality indexes from Sentinel-2 imagery: development and validation around Italian river estuaries. In *Geophysical Research Abstracts* (Vol. 20).

Osei, L. K., Asmah, R., Aikins, S., & Karikari, A. Y. (2019). Effects of Fish Cage Culture on Water and Sediment Quality in the Gorge Area of Lake Volta in Ghana: A Case Study of Lee Fish Cage Farm. *Ghana Journal of Science, 60*(1), 1–16. https://doi.org/10.4314/gjs.v60i1.1

PAGASA (2023, February). ANNUAL REPORT ON PHILIPPINE TROPICAL CYCLONES 2020. PAGASA Public Files. Retrieved from https://pubfiles.pagasa.dost.gov.ph/pagasaweb/files/tamss/weather/tcsummary/PAGASA_ARTC_2020.pdf

Perrone, M., Scalici, M., Conti, L., Moravec, D., Kropáček, J., Sighicelli, M., Lecce, F., & Malavasi, M. (2021). Water Mixing Conditions Influence Sentinel-2 Monitoring of Chlorophyll Content in Monomictic Lakes. *Remote Sensing, 13*(14), 2699. https://doi.org/10.3390/rs13142699

Pisanti, A., Magrì, S., Ferrando, I., & Federici, B. (2022). SEA WATER TURBIDITY ANALYSIS FROM SENTINEL-2 IMAGES: ATMOSPHERIC CORRECTION AND BANDS CORRELATION. *The International Archives of the Photogrammetry, Remote Sensing and Spatial Information Sciences, XLVIII-4/W1-2022*, 371–378. https://doi.org/10.5194/isprs-archives-XLVIII-4-W1-2022-371-2022

Sebastiá-Frasquet, M.-T., Aguilar-Maldonado, J. A., Santamaría-Del-Ángel, E., & Estornell, J. (2019). Sentinel 2 Analysis of Turbidity Patterns in a Coastal Lagoon. *Remote Sensing, 11(24)*, 2926. https://doi.org/10.3390/rs11242926

Sulekan, A., & Syed Jamaludin, S.S. (2020). Review on Geographically Weighted Regression (GWR) approach in spatial analysis. *Malaysian Journal of Fundamental and Applied Sciences. 16*. 173-177. https://doi.org/10.11113/mjfas.v16n2.1387.

Swenson, H., Baldwin, H., & Cordy, G. (2018, June 6). Turbidity and Water | U.S. Geological Survey. USGS.gov. Retrieved from https://www.usgs.gov/special-topics/water-science-school/science/turbidity-and-water#overview

Vanhellemont, Q., & Ruddick, K. (2016). *ACOLITE processing for Sentinel-2 and Landsat-8: atmospheric correction and aquatic applications*.

Vanhellemont, Q., & Ruddick, K. (2018). Atmospheric correction of metre-scale optical satellite data for inland and coastal water applications. *Remote Sensing of Environment, 216*, 586–597. https://doi.org/10.1016/j.rse.2018.07.015

Zainurin, S. N., Wan Ismail, W. Z., Mahamud, S. N. I., Ismail, I., Jamaludin, J., Ariffin, K. N. Z., & Wan Ahmad Kamil, W. M. (2022). Advancements in Monitoring Water Quality Based on Various Sensing Methods: A Systematic Review. *International journal of environmental research and public health, 19(21)*, 14080. https://doi.org/10.3390/ijerph192114080